Extensive MIS 3 glaciation in southernmost Patagonia revealed by cosmogenic nuclide dating of outwash sediments

Christopher M. Darvill [a,b,∗], Michael J. Bentley [a], Chris R. Stokes [a], Andrew S. Hein [c], Ángel Rodés [d]

[a] Department of Geography, Durham University, South Road, Durham, DH1 3LE, UK
[b] British Antarctic Survey, Madingley Road, Cambridge, CB3 0ET, UK
[c] School of Geosciences, University of Edinburgh, Drummond Street, Edinburgh, EH8 9XP, UK
[d] Scottish Universities Environmental Research Centre, East Kilbride, G75 0QF, UK

ABSTRACT

The timing and extent of former glacial advances can demonstrate leads and lags during periods of climatic change and their forcing, but this requires robust glacial chronologies. In parts of southernmost Patagonia, dating pre-global Last Glacial Maximum (gLGM) ice limits has proven difficult due to post-deposition processes affecting the build-up of cosmogenic nuclides in moraine boulders. Here we provide ages for the Río Cullen and San Sebastián glacial limits of the former Bahía Inútil–San Sebastián (BI-SSb) ice lobe on Tierra del Fuego (53–54°S), previously hypothesised to represent advances during Marine Isotope Stages (MIS) 12 and 10, respectively. Our approach uses cosmogenic ^{10}Be and ^{26}Al exposure dating, but targets glacial outwash associated with these limits and uses depth-profiles and surface cobble samples, thereby accounting for surface deflation and inheritance. The data reveal that the limits formed more recently than previously thought, giving ages of 45.6 ka ($+139.9/−14.3$) for the Río Cullen, and 30.1 ka ($+45.6/−23.1$) for the San Sebastián limits. These dates indicate extensive glaciation in southern Patagonia during MIS 3, prior to the well-constrained, but much less extensive MIS 2 (gLGM) limit. This suggests the pattern of ice advances in the region was different to northern Patagonia, with the terrestrial limits relating to the last glacial cycle, rather than progressively less extensive glaciations over hundreds of thousands of years. However, the dates are consistent with MIS 3 glaciation elsewhere in the southern mid-latitudes, and the combination of cooler summers and warmer winters with increased precipitation, may have caused extensive glaciation prior to the gLGM.

1. Introduction

The terrestrial record of former southern hemisphere ice masses has been used to assess inter-hemispheric synchroneity of glacial advance and retreat (Sugden et al., 2005) and how climatic forcing, such as changes in the Southern Westerly Winds (Fig. 1), triggered ice growth or decay through time. Patagonia is an ideal location for such records because it spans a large latitudinal range and exhibits well-preserved glacial geomorphology reflecting former advances of the Patagonian Ice Sheet (Clapperton, 1993; Rabassa, 2008; Sugden et al., 2005). However, coupling glacial reconstructions with robust chronologies can be challenging.

The established model for the timing of glaciations in this region is that, following the 1.1 Ma Greatest Patagonian Glaciation (Caldenius, 1932; Mercer, 1983), ice lobes oscillated in unison, creating a pattern of 'nested' glacial limits resulting from a series of progressively less-extensive glaciations throughout the Quaternary (Coronato et al., 2004). Chronologies from northern Patagonia have demonstrated such a pattern (Hein et al., 2009, 2011; Kaplan et al., 2005, 2009; Singer et al., 2004), but the timing of glacial advances in southernmost Patagonia is more conjectural. On Tierra del Fuego (53–54°S), moraines hypothesised to have been deposited during MIS 12 (*ca.* 450 ka) and MIS 10 (*ca.* 350 ka) have been dated using cosmogenic nuclide exposure dating of erratic boulders and yielded dates ranging from 15 to 224 ka, and centred around *ca.* 21 ka, similar to the LGM limit (Fig. 1; Evenson et al., 2009; Kaplan et al., 2007). It has been suggested that this could be due to intense post-depositional exhumation and erosion of the boulders from MIS 12/10 limits (Kaplan et al., 2007), but an alternative
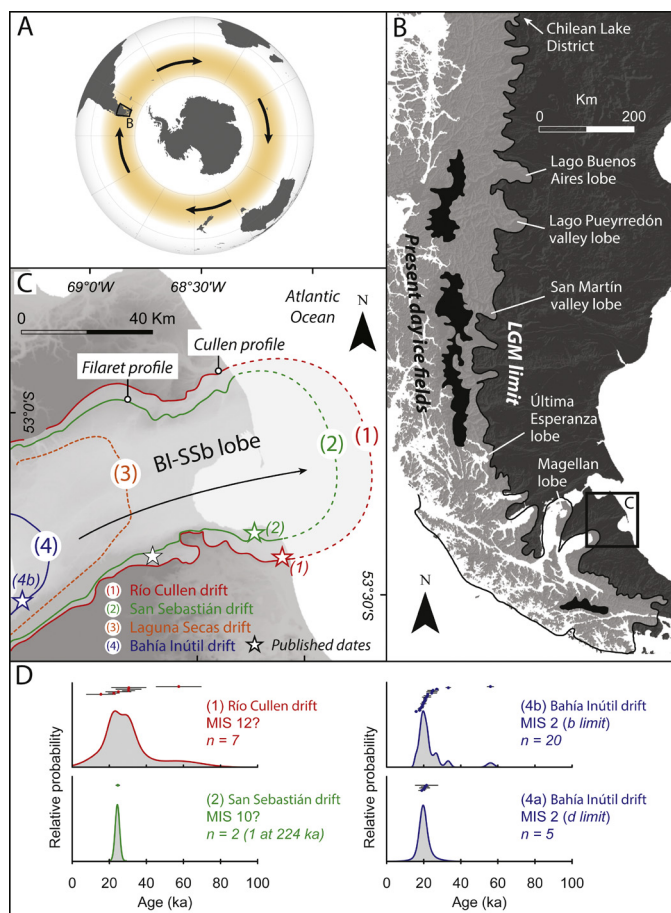
Fig. 1. (A) Location of the study area, with shading indicating the approximate present extent of the Southern Westerly Wind system. (B) Map of Patagonia with LGM ice extent from Singer et al. (2004) and locations mentioned in the text. (C) Drift limits of the former Bahía Inútil–San Sebastián ice lobe across northern Tierra del Fuego. Dashed lines indicate inferred extents (Rabassa, 2008). Stars show approximate locations of previously published ^{10}Be dates from boulder trains (McCulloch et al., 2005b; Kaplan et al., 2007, 2008; Evenson et al., 2009), and the Filaret and Cullen depth profiles from this study are labelled. The Bahía Inútil drift (4) correlates with the gLGM. (D) Previously published ^{10}Be moraine boulder exposure dates from the study area, shown as cumulative probability density function plots and as data points with associated errors, recalculated using the New Zealand production rate (Putnam et al., 2010). Graphs are labelled according to drift limits in C, along with the published hypothesised MIS age and the number of samples. One additional exposure date for limit 2 is 224 ± 7 ka.

hypothesis, suggested here, is that the dates are closer to the true age of the glacial advance whereby, following the Greatest Patagonian Glaciation, the ice lobe was most extensive during the last glacial cycle (MIS 4-2).

In this study, we test these two opposing hypotheses using a new method that can account for post-depositional processes. Specifically, Hein et al. (2009) demonstrated that cosmogenic nuclide depth-profiles through outwash associated with moraine limits can yield robust ages for glacial limits where post-depositional erosion and exhumation may compromise traditional moraine-boulder samples. We present ^{10}Be and ^{26}Al dates from two depth profiles through outwash associated with glacial limits of the Bahía Inútil–San Sebastián (BI-SSb) ice lobe on Tierra del Fuego and use these results to test the established age model for the timing of glacial advance.

2. Study area and existing chronology

The BI-SSb depression in central Tierra del Fuego was the former location of an eastward flowing ice-lobe sourced from the

Cordillera Darwin range to the southwest (Fig. 1; Darvill et al., 2015; Evenson et al., 2009). The LGM limit of the BI-SSb lobe is well-dated: radiocarbon, amino-acid racemisation, tephrostratigraphy and cosmogenic nuclide exposure dating have all been conducted on moraines or associated deposits around Bahía Inútil (Clapperton et al., 1995; Evenson et al., 2009; Kaplan et al., 2008; McCulloch et al., 2005a, 2005b; Meglioli, 1992; Rutter et al., 1989). The consistency amongst these dating techniques leaves little uncertainty that this limit was deposited during the global LGM (gLGM: 26.5 to 19 ka; Clark et al., 2009).

More problematic are the three older, nested limits of greater extent than the gLGM. The most comprehensive study of these limits was produced by Meglioli (1992), in which an age model was hypothesised for the Laguna Secas (MIS 6), San Sebastián (MIS 10) and Río Cullen (MIS 12) drift limits. The model was based on weathering analysis and correlation with similar patterns of nested limits further north that had been ^{40}Ar/^{39}Ar and K–Ar dated (Fig. 1; Meglioli, 1992; Mercer, 1983; Singer et al., 2004). There are no dates to support the age of the Laguna Secas limit, but the two large bands of kettle and kame drift that correspond with the San Sebastián and Río Cullen limits have been dated (Figs. 1 and 2). The inner, San Sebastián, drift is hypothesised to date from MIS 10 based on correlations to Uranium-series dated marine terraces (Bujalesky et al., 2001; Coronato et al., 2004). The outer, Río Cullen, drift is hypothesised to date from MIS 12 (Coronato et al., 2004) based on ages of <760 ka derived from palaeomagnetic measurements of basal till (Walther et al., 2007). However, direct cosmogenic nuclide exposure dating of boulders on both drifts yielded substantially younger ages ranging from 15 to 224 ka, with most <100 ka (Fig. 1; Evenson et al., 2009; Kaplan et al., 2007). Given this spread of ages, it is worth explaining the basis of the published interpretation of these deposits.

Three raised marine terraces exist on the east coast of Tierra del Fuego, south of the former BI-SSb lobe, and have been hypothesised to represent three marine transgressions during MIS 11, 7–9 and 5 (Bujalesky et al., 2001). However, Uranium-series dating of the MIS 11 and 7–9 terraces yielded ambiguous results and the MIS 5 terrace has only been radiocarbon dated, using shells, to 43 ka B.P. (Codignotto and Malumian, 1981). Rutter et al. (1989) and Meglioli (1992) also conducted amino-acid racemisation on shells from this terrace, and suggested that the D/L aspartic acid ratios most likely correspond with MIS 5e. Again, Uranium-series dating of shells from the terrace was problematic, but the best 'apparent' age was 82 ka (Bujalesky et al., 2001). Although none of these terraces extend into the area occupied by the BI-SSb lobe, Bujalesky et al. (2001) suggested that the terraces are all incised into the lower of two glaciofluvial fans relating to outwash from the San Sebastián drift (upper fan) and Río Cullen drift (lower fan). Consequently, they inferred that the Río Cullen drift must be older than the highest terrace (inferred to be MIS 11), although the morphostratigraphic link is not altogether clear and our mapping was not able to trace unambiguously the outwash from the fans back to the respective moraine limits.

The only direct dating for the Río Cullen and San Sebastián limits has been palaeomagnetic analysis of till and cosmogenic nuclide exposure dating of moraine boulders. Both limits are thought to be <760 ka because Walther et al. (2007) found basal till sediments at the coast in the Río Cullen drift to be normally polarised and assigned them to the Brunhes chron. Using cosmogenic nuclides for exposure dating, Kaplan et al. (2007) and Evenson et al. (2009) found ages almost entirely <100 ka (and dominantly <50 ka) for boulders on both limits. These were rejected by the authors as too young based on the indirect dating outlined above and because the boulders showed extensive erosion that could have artificially reduced the ages (Kaplan et al., 2007). Importantly, similar boulder dating from the Magellan and Bella Vista (also known as 'Río
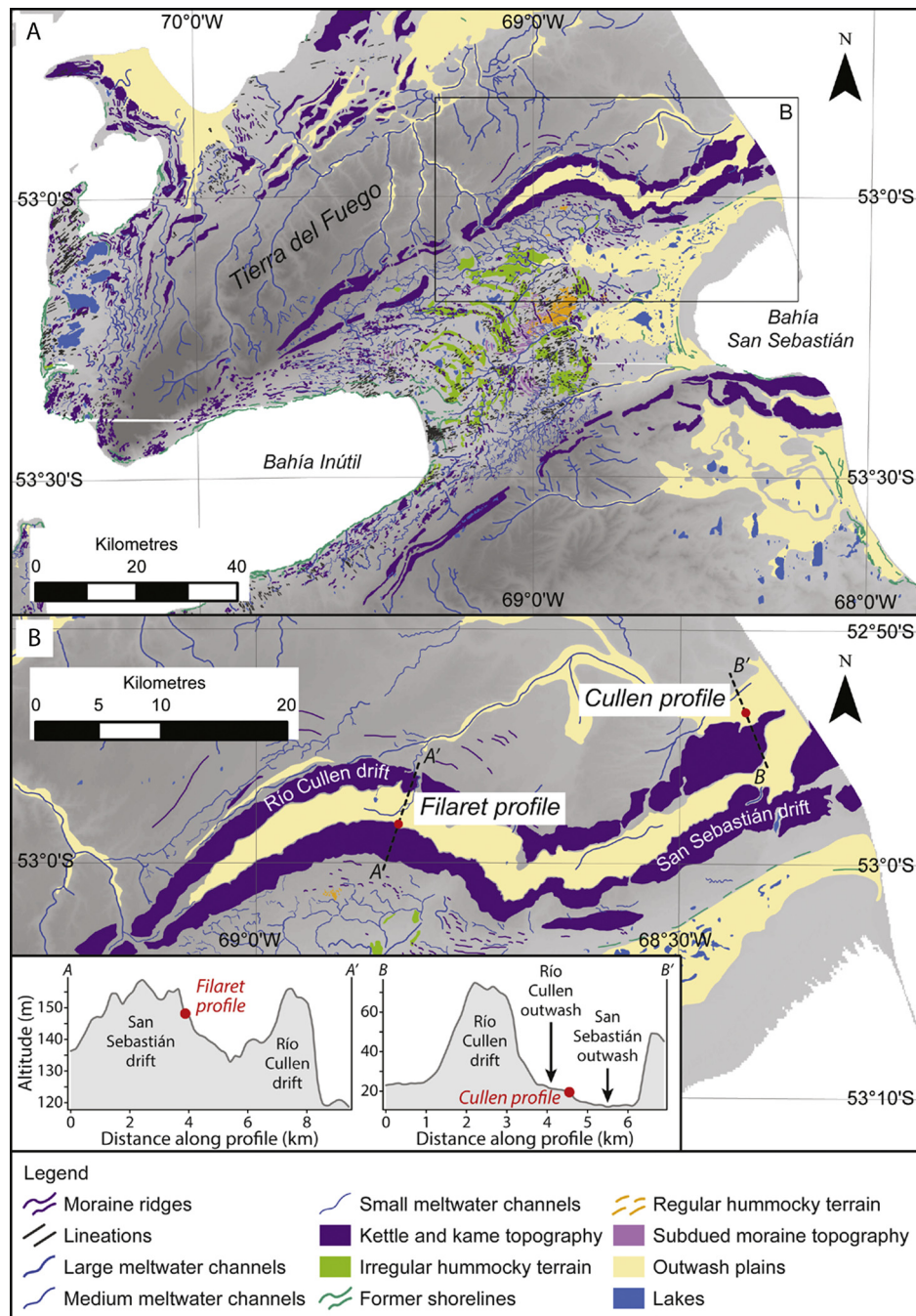
Fig. 2. (A) The glacial geomorphology of the former BI-SSb ice lobe in Tierra del Fuego, adapted from Darvill et al. (2014). (B) An enlarged version of the map showing the locations of the Cullen and Filaret profiles sampled in this study. Also shown are topographic profiles for transects A–A′ and B–B′ across the glacial drift limits and sampled outwash.

Gallegos' or 'Ultíma Esperanza') lobes to the north also gave ages younger than anticipated (Kaplan et al., 2007). Unlike the BI-SSb lobe, some of the Magellan and Bella Vista glacial limits have been independently constrained using $^{40}Ar/^{39}Ar$ and K–Ar dating of lava flows interbedded with tills (Meglioli, 1992; Mercer, 1983; Singer et al., 2004). This lends support to the rejection of boulder ages from all ice lobes in the region due to post-depositional processes (Kaplan et al., 2007), in a manner similar to that reported by Hein et al. (2009) for the Pueyrredón lobe. Despite the published interpretation, we argue that the ages of the Río Cullen and San Sebastián limits remain unclear, and an alternative approach to cosmogenic nuclide exposure dating of boulders in the region is required.

3. Methods

3.1. Sampling

We identified locations where the Río Cullen and San Sebastián limits could be linked unequivocally to their associated outwash units. An overview of the glacial geomorphology of this part of Tierra del Fuego is shown in Fig. 2. The outwash has been mapped unambiguously to the glacial limits in question (Darvill et al., 2014) and, in both cases, it was possible to walk directly from the sample locations on the outwash surfaces onto the kettle kame drift deposits of the glacial limits.

Fig. 3. (A) Photograph of the Cullen depth profile during sampling. The top of the profile was taken from the local soil level, given there was some spoil from the quarry. (B) and (C) Photographs of two of the surface cobble samples from the Cullen profile labelled with sample names and calculated ^{10}Be/^{26}Al ages (respectively). (D) Photograph of the Filaret depth profile during sampling. (E) and (F) Photographs of two of the surface cobble samples from the Filaret profile labelled with sample names and calculated ^{10}Be/^{26}Al ages (respectively). Further panoramic sketches, sedimentary logs and sampling photographs can be found in the Supplementary Material.

The outwash surfaces retained original surface morphology and appeared to be relatively undisturbed. The path of meltwater issuing from the inner San Sebastián glacial limit could be clearly traced through the outer Río Cullen glacial limit, and formed an incised channel in the Río Cullen outwash surface that did not affect the Río Cullen sampling (Fig. 2 and see Supplementary Material). Furthermore, meltwater younger than the San Sebastián glacial limit was topographically confined to the central BI-SSb depression (Fig. 2), where it flowed directly east toward the Atlantic. Two depth profiles were sampled at these locations, relating to the San Sebastián glacial limit (Filaret profile) and the Río Cullen glacial limit (Cullen profile). The surfaces of these units possessed a well preserved morphology (e.g. braided meltwater channels), graded directly to the moraines of the drift limit, and showed no evidence of post-depositional reworking. Consequently, they are ideal locations for dating using outwash depth-profiles (Hein et al., 2009, 2011).

The depth profiles were sampled from exposures within small, contemporary road-side quarries. These were cleared and logged, exhibiting sediments ranging from silts to cobbles of various mixed lithologies (Fig. 3 and see Supplementary Material). Our field observations suggested that each outwash terrace accumulated continuously as a discrete deposit associated with the meltwater issuing from the nearby glacial limit. Both were covered in low grass and were capped by brown, silty, poorly-developed soils up to ∼25 cm deep. Each contained a single outwash unit of silts, sands, gravels and cobbles at various grades, but with no obvious signs that their source had changed over time. There were no frost wedges within the sediments and no clear signs of cryoturbation or pedogenic carbonate formation. Depths through the outwash

were measured with a tape measure from the surface and were demarcated for sampling using a spirit level and spray-paint. We followed Hein et al. (2009) in collecting depth and surface samples to allow modelling of cosmogenic ^{10}Be and ^{26}Al accumulation to give a most probable unit age, whilst constraining inheritance and post-depositional surface erosion.

Small (ca. 6 cm) quartz cobbles embedded within the outwash surface in the vicinity of the exposures were sampled, crushed whole, and analysed individually as independent estimates of surface exposure time. We also collected ∼1 kg samples of mixed lithology pebbles (>0.5 cm and <4 cm) at 25 cm depth intervals (depth error ≤4 cm), including a sample at the base of the section to help calculate inheritance in the profile. Each depth sample was amalgamated and analysed for ^{10}Be and ^{26}Al concentrations. One sample (FP025cs) consisted half of sand matrix due to insufficient clasts at that depth. In both profiles the lowermost sample consisted of two separate depth samples combined (i.e. an unprocessed weight of ∼2 kg) due to insufficient quartz; hence the apparent thickness represented by these samples is greater. Detailed sample information is given in Table 1.

The nuclide concentration data from the depth profile samples were modelled to yield most probable age, erosion rate and inheritance estimates for the outwash unit. The surface cobble samples were treated independently as exposure age estimates for the outwash surface.

3.2. Chemical analysis

All physical and chemical preparation and ^{10}Be/^{9}Be and ^{26}Al/^{27}Al AMS measurements were carried out at the Scottish Univer-

Table 1
Sample descriptions and nuclide concentrations.

Be ID	Al ID	Type[a]	Sample ID	Latitude (DD)	Longitude (DD)	Altitude (m asl)	Elv. flag	Thickness (cm)[b]	Density (g cm^{-2})[c]	Shielding correction	Erosion (cm yr^{-1})	^{10}Be (atoms g^{-1})	1σ (atoms g^{-1})	Be AMS std	^{26}Al (atoms g^{-1})	1σ (atoms g^{-1})	Al AMS std
Filaret profile																	
b6888	a1765	a	FP025CS	−52.9743	−68.8310	148	std	4	–	0.999999	0	123,056	5543	NIST_27900	923,474	34,485	Z92-0222
b6889	a1766	a	FP050	−52.9743	−68.8310	148	std	4	–	0.999999	0	108,030	4819	NIST_27900	756,901	35,858	Z92-0222
b6890	a1767	a	FP100	−52.9743	−68.8310	148	std	4	–	0.999999	0	72,733	3034	NIST_27900	461,039	17,810	Z92-0222
b6891	a1768	a	FP125	−52.9743	−68.8310	148	std	4	–	0.999999	0	61,958	2861	NIST_27900	382,692	15,694	Z92-0222
b6892	a1769	a	FP150	−52.9743	−68.8310	148	std	4	–	0.999999	0	38,461	1812	NIST_27900	306,046	11,766	Z92-0222
b6894	a1771	a	FP200230	−52.9743	−68.8310	148	std	34	–	0.999999	0	50,200	3342	NIST_27900	347,187	22,568	Z92-0222
b6895	a1772	s	FPSS1	−52.9743	−68.8310	148	std	6	2.7	0.999999	0	127,390	3653	NIST_27900	856,986	29,261	Z92-0222
b6896	a1773	s	FPSS12	−52.9743	−68.8310	148	std	6	2.7	0.999999	0	118,438	4222	NIST_27900	792,773	35,652	Z92-0222
b6897	a1774	s	FPSS13	−52.9743	−68.8310	148	std	6	2.7	0.999999	0	131,073	5696	NIST_27900	819,874	26,226	Z92-0222
b6898	a1775	s	FPSS16	−52.9743	−68.8310	148	std	6	2.7	0.999999	0	118,430	4081	NIST_27900	860,572	36,911	Z92-0222
Cullen profile																	
b6903	a1778	a	CP025	−52.8899	−68.4244	17	std	4	–	0.999999	0	111,182	5361	NIST_27900	840,414	31,669	Z92-0222
b6904	a1819	a	CP050	−52.8899	−68.4244	17	std	4	–	0.999999	0	101,669	6596	NIST_27900	738,532	32,418	Z92-0222
b6905	a1779	a	CP075	−52.8899	−68.4244	17	std	4	–	0.999999	0	154,494	5576	NIST_27900	1,095,953	37,862	Z92-0222
b6906	a1780	a	CP100	−52.8899	−68.4244	17	std	4	–	0.999999	0	85,944	3075	NIST_27900	579,643	21,486	Z92-0222
b6908	a1820	a	CP150	−52.8899	−68.4244	17	std	4	–	0.999999	0	58,815	2940	NIST_27900	359,452	15,955	Z92-0222
b6909	a1821	a	CP250275	−52.8899	−68.4244	17	std	29	–	0.999999	0	72,573	3981	NIST_27900	550,438	23,670	Z92-0222
b6910	a1781	s	CPSS5	−52.8899	−68.4244	17	std	6	2.7	0.999999	0	180,591	4619	NIST_27900	868,057	29,274	Z92-0222
b6911	a1782	s	CPSS7	−52.8899	−68.4244	17	std	6	2.7	0.999999	0	99,630	2922	NIST_27900	784,025	27,306	Z92-0222
b6912	a1784	s	CPSS8	−52.8899	−68.4244	17	std	6	2.7	0.999999	0	112,414	3101	NIST_27900	806,137	29,141	Z92-0222
b7197	a1785	s	CPSS14	−52.8899	−68.4244	17	std	6	2.7	0.999999	0	130,107	3377	NIST_27900	918,950	33,591	Z92-0222

[a] a – amalgamated depth profile sample; s – individual surface cobble sample.
[b] Depth sample thickness set at a standard 4 cm error, with amalgamated samples including the depth between samples; surface cobble samples set at a standard 6 cm error.
[c] Surface sample density is estimated at 2.7 g cm^{-3}; depth samples density is constrained during modelling.

sities Environmental Research Centre (SUERC) as part of the NERC Cosmogenic Isotope Analysis Facility (CIAF), as per Wilson et al. (2008).

Surface cobbles were treated individually, whereas depth samples were treated as amalgams. All samples were crushed whole, milled and sieved, and the >125 μm to <500 μm fraction was then magnetically separated using a Frantz machine prior to chemical analysis. They were treated with a 2:1 mixture of H_2SiF_6 and HCl on a shaker table to dissolve non quartz minerals. The quartz was then purified by repeat etching in HF on a shaker table to remove >30% of the starting mass; with the ion concentration gauged using assays measured by ICP-OES.

All samples were dissolved in 40% HF dry-downs on a hotplate. 0.2 mg of ^{9}Be carrier was added to each sample and ^{26}Al carrier was added to most samples so that 2 mg of Al per sample was reached. The solutions were passed through anion exchange columns to remove Fe and other contaminants, and then precipitated to remove Ti prior to being passed through cation exchange columns to separate Be and Al. The separate Be and Al fractions were precipitated and converted to BeO and Al_2O_3, before being prepared for AMS analysis.

NIST-SRM4325 and PRIME-Z93-0005 primary standards were used for AMS measurements, with nominal ratios of 2.97×10^{-11} ^{10}Be/^{9}Be and 4.11×10^{-11} ^{26}Al/^{27}Al, respectively. The reported uncertainties of the nuclide concentrations include 2.5% for the AMS and chemical preparation. Blank corrections ranged between 3 and 15% of the sample ^{10}Be/^{9}Be ratios and between 0 and 0.9% of the sample ^{26}Al/^{27}Al ratios. The uncertainty of the blank measurements is included in the stated uncertainties. All nuclide concentration data are given in Table 1.

3.3. Age determination

3.3.1. Scaling scheme and production rate

For consistency, the time-dependent scaling scheme of Lal (1991) and Stone (2000) was used in surface sample age calibrations and recalibrations of published data. Likewise, the production rate of Putnam et al. (2010) from New Zealand was used throughout to calibrate ^{10}Be and ^{26}Al measurements, given that it is now in common use in Patagonia and the southern hemisphere and that it overlaps at 1σ with an independent production rate from Lago Argentino in Patagonia (Kaplan et al., 2011). We assessed the implications of choosing this production rate and scaling scheme combination using our surface sample ages calculated using the New Zealand production rate and the Lal (1991) and Stone (2000) time-dependent scaling scheme. The global production rate gave ages <17% younger than our ages (irrespective of scaling scheme) but the Patagonian production rate gave ages <6% older or younger than our ages (irrespective of scaling scheme) or <5% older or younger when the same scaling schemes were compared. Using the New Zealand production rate, altering the scaling scheme resulted in <3% older or younger ages. Our choice of production rate and scaling scheme does not alter our conclusions.

3.3.2. Surface samples

Apparent ^{10}Be and ^{26}Al exposure ages and internal uncertainties from surface sample measurements were calculated using the CRONUS-earth online calculator version 2.2 (available at http://hess.ess.washington.edu/math/; Wrapper script: 2.2; Main calculator: 2.1; Objective function: 2; Constants: 2.2.1; Muons: 1.1; see Balco et al., 2008). We assumed a density of 2.7 g cm^{-3} (equivalent to the density of pure quartz) and used a standard, excess thickness of 6 cm for all samples to correct for self-shielding. Topographic shielding was measured in the field using an abney level but this correction was minimal (scaling factor >0.999999). Present day snow and vegetation cover is thin, and is unlikely to

have increased significantly during glacial times, so no correction was applied for shielding by snow cover or vegetation. Likewise, no erosion correction was applied given that the quartz cobbles showed no significant signs of surface erosion. As a result of these assumptions, the ages should be considered minimum estimates.

3.3.3. Depth profiles

The concentration data from the depth samples were modelled using Hidy et al. (2010; version 1.2). The model was designed to compute cosmogenic nuclide concentrations through sedimentary depth profiles by applying Monte Carlo simulations whilst accounting for uncertainties. It can be constrained using geological parameters to produce a most probable surface exposure age, erosion rate and nuclide inheritance estimate for each outwash unit. For both depth profiles, there were samples that deviated from the theoretical nuclide decay curve: FP150 for the Filaret profile and CP75 and CP150 for the Cullen profile. We used a jack-knifing process to test whether these were outliers by running the model with wide parameters and then excluding all of the samples one at a time. The model would only run with the outliers mentioned above removed from the profiles and they were not included in further modelling. This resulted in normally decreasing nuclide concentrations with depth, though the modelling was constrained by fewer samples.

The ^{26}Al/^{10}Be ratio for CP150 plotted well below the steady state erosion island, normally indicative of a period of burial that results in a lower ^{26}Al/^{10}Be ratio. However, it is unclear why the FP150 and CP75 samples yielded anomalous results, given that the ^{26}Al/^{10}Be ratios are not low. Furthermore, there is no evidence for changing sedimentary processes at any of these three depths. Alternatively, anomalous results could have been caused by issues with the physical or chemical preparation of these samples, though no issues were recorded at the time and it is not possible to state the exact cause. With only four samples in the Cullen profile, the model yielded weaker constraint in the final age estimates.

There are two potential issues with using the Monte Carlo approach of Hidy et al. (2010) for our profile samples. First, it may artificially create a maximum age for a profile if the upper age-erosion rate area is narrow (Rodés et al., 2014). Secondly, without constraint on either erosion rate or age, our profiles may only yield minimum ages (see Hidy et al., 2010). We addressed the first issue by comparing initial results (from model runs with wide parameters) with an alternative model by Rodés et al. (2014). Both the Hidy et al. (2010) and the Rodés et al. (2014) models gave similar results despite modelling the ages in different ways, suggesting that our data yielded minimum and maximum ages. We then continued modelling using the Hidy et al. (2010) model because it allows the user to constrain geological input parameters. We tackled the second issue by running sensitivity tests and also applying *a priori* knowledge to constrain the model parameters. We discuss the nature of these constraints in more detail in Section 4.2.

4. Results

4.1. Surface sample results

The four Río Cullen surface sample ^{10}Be exposure ages range from 23.7 to 43.2 ka (Table 2). The oldest sample (CPSS5) yielded a ^{26}Al/^{10}Be ratio below the steady state erosion island, indicating a complex exposure-burial history (Fig. 4). Removing this outlier reduces the range to 23.7 to 31.0 ka ($n = 3$). The four San Sebastián surface sample ^{10}Be exposure ages are tightly clustered, ranging from 24.7 to 27.4 ka ($n = 4$), with all samples showing ^{26}Al/^{10}Be ratios consistent with a simple exposure history (Fig. 4).

Table 2
Calculated ages for surface samples using CRONUS-Earth calculator (Balco et al., 2008). Grey shading indicates the production rate and scaling scheme used.

Sample ID	P_NZ										P_PTGN		P_GLOBAL		P_NZ	
	St		De		Du		Li		Lm		Lm		Lm		Lm	
	age (a)	±	age (a)	±	age (a)	±	age (a)	±	age (a)	±	age (a)	±	age (a)	±	age (a)	±
Filaret profile																
Be																
FPSS1	26,050	944	26,824	964	27,102	974	26,387	940	26,633	961	26,260	1163	22,871	2048	**26,633**	**961**
FPSS12	24,208	1017	24,933	1041	25,197	1052	24,544	1019	24,750	1036	24,404	1199	21,256	1956	**24,750**	**1036**
FPSS13	26,808	1312	27,603	1345	27,885	1358	27,145	1316	27,407	1338	27,024	1491	23,536	2245	**27,407**	**1338**
FPSS16	24,206	992	24,931	1016	25,195	1026	24,542	993	24,749	1011	24,403	1178	21,255	1946	**24,749**	**1011**
Al																
FPSS1	25,892	1062	26,660	1086	26,936	1098	26,229	1062	26,469	1082	26,088	1264	22,741	2091	**26,469**	**1082**
FPSS12	23,929	1210	24,643	1241	24,905	1254	24,265	1216	24,463	1234	24,111	1368	21,021	2029	**24,463**	**1234**
FPSS13	24,757	969	25,494	992	25,762	1002	25,093	969	25,309	987	24,945	1169	21,747	1982	**25,309**	**987**
FPSS16	26,001	1267	26,773	1299	27,049	1312	26,339	1271	26,582	1292	26,199	1444	22,838	2184	**26,582**	**1292**
Cullen profile																
Be																
CPSS5	42,169	1431	43,052	1447	43,388	1458	42,272	1407	43,215	1459	42,609	1811	37,095	3298	**43,215**	**1459**
CPSS7	23,154	850	23,669	862	23,936	872	23,358	844	23,704	867	23,373	1044	20,364	1827	**23,704**	**867**
CPSS8	26,145	925	26,717	937	27,007	947	26,332	915	26,769	942	26,396	1150	22,995	2051	**26,769**	**942**
CPSS14	30,291	1034	30,944	1046	31,257	1057	30,457	1020	31,022	1053	30,588	1303	26,643	2365	**31,022**	**1053**
Al																
CPSS5	29,862	1216	30,505	1235	30,815	1247	30,031	1207	30,580	1241	30,140	1454	26,275	2416	**30,580**	**1241**
CPSS7	26,933	1121	27,519	1138	27,812	1150	27,117	1114	27,575	1144	27,179	1331	23,699	2187	**27,575**	**1144**
CPSS8	27,703	1185	28,304	1204	28,601	1216	27,883	1178	28,365	1210	27,957	1397	24,376	2262	**28,365**	**1210**
CPSS14	31,640	1367	32,318	1389	32,638	1402	31,800	1358	32,404	1396	31,937	1608	27,839	2593	**32,404**	**1396**

Production rates: P_{NZ} – New Zealand production rate of Putnam et al. (2010); P_{PTGN} – Patagonian production rate of Kaplan et al. (2011); P_{GLOBAL} – global production rate of Balco et al. (2008) and Nishiizumi et al. (2007). Scaling schemes: Lm – time-dependent version of Lal (1991) and Stone (2000); see Supplementary Material for other scaling schemes.

4.2. Depth profile modelling

There is a paradox involved in modelling cosmogenic nuclide depth profiles. Often, parameters are unknown, but models require some constraint to produce an age. In theory, very wide, even unrealistic, parameters will yield the most reliable estimates of age, erosion rate and inheritance. However, the wider the constraints, the slower the model will run (if at all) and the wider the resulting error ranges. Consequently, a balance must be found between applying constraints to aid modelling and not inadvertently constraining the age, erosion rate and inheritance without good reason. In this section, we outline the conservative constraints that we applied to the Hidy et al. (2010) model. We present χ^2 sensitivity tests to check that the model output was not inadvertently affected and discuss where there is good reason to apply constraint based on *a priori* knowledge. Model parameters are given in Table 3 and a summary of the [10]Be depth profile results is given in Table 4, with detailed results in the Supplementary Material.

4.2.1. Sensitivity tests

χ^2 sensitivity tests were conducted whereby broad model parameters were used (Table 3) and a single controlling parameter was then varied with each model run (see Supplementary Information for sensitivity results). Importantly, the controlling parameters only reduced the χ^2 maximum age, and did not significantly affect the χ^2 optimum or minimum age estimates. The sensitivity tests demonstrated that there were three model parameters which controlled the χ^2 maximum ages: *maximum total erosion*, *maximum age*, and *inheritance*. Of these, the *maximum total erosion* is the key determinant given that *maximum age* can be constrained to *ca.* 1100 ka by independent dating of the Greatest Patagonian Glaciation across Patagonia (Meglioli, 1992; Singer et al., 2004) and *inheritance* can be constrained using the deepest samples. The *maximum total erosion* parameter differs from the *erosion rate* parameter in that the former is a threshold depth of erosion that the model is not permitted to exceed, regardless of the erosion rate or age of the sedimentary unit.

4.2.2. Density

Density through the profiles was unknown, and could not be measured in the field. However, it is an important age determinant in profile modelling, especially as most models behave according to the time-averaged density, rather than the present density (Rodés et al., 2011). We ran sensitivity tests with very wide constraints (between 1 and 3 g cm^{-3}) and then used the change in maximum age outputs to constrain values slightly, though these were still extremely conservative given the nature of the sediments (between 1 and 2.7 g cm^{-3}).

4.2.3. Inheritance

Inheritance was essentially unknown. We ran sensitivity tests to assess the effect of inheritance on maximum age outputs and then selected wide constraints. Given that we had deep samples in both profiles, we could also back-check the modelled inheritance in all model runs with the deep-sample nuclide concentrations. In all cases, our maximum inheritance parameters were well in excess of the measured deep nuclide concentrations.

4.2.4. Age limits

Initial modelling in conjunction with the Rodés et al. (2014) model gave maximum ages far older (5000 ka for the Filaret profile and 4000 ka for the Cullen profile) than the known age of the Greatest Patagonian Glaciation at 1100 ka (Meglioli, 1992; Singer et al., 2004). We used these extreme upper limits for sensitivity tests and then took 1100 ka as a more reasonable, but still highly conservative, maximum age limit for all other modelling. We applied no lower age limit during sensitivity tests, but then used an age of 14.3 ka for all other modelling. This is from a well dated Reclus tephra layer, known to have been deposited after the deposition of the gLGM glacial limit close to Bahía Inútil (McCulloch et al., 2005b; Wastegård et al., 2013) and is only used to prevent a stratigraphic age reversal for the Cullen profile due to it containing fewer depth samples. Again, this is highly conservative, particularly as radiocarbon dating by Hall et al. (2013) suggested that ice had retreated into the fjords of Cordillera Darwin by *ca.* 16.8 ka.
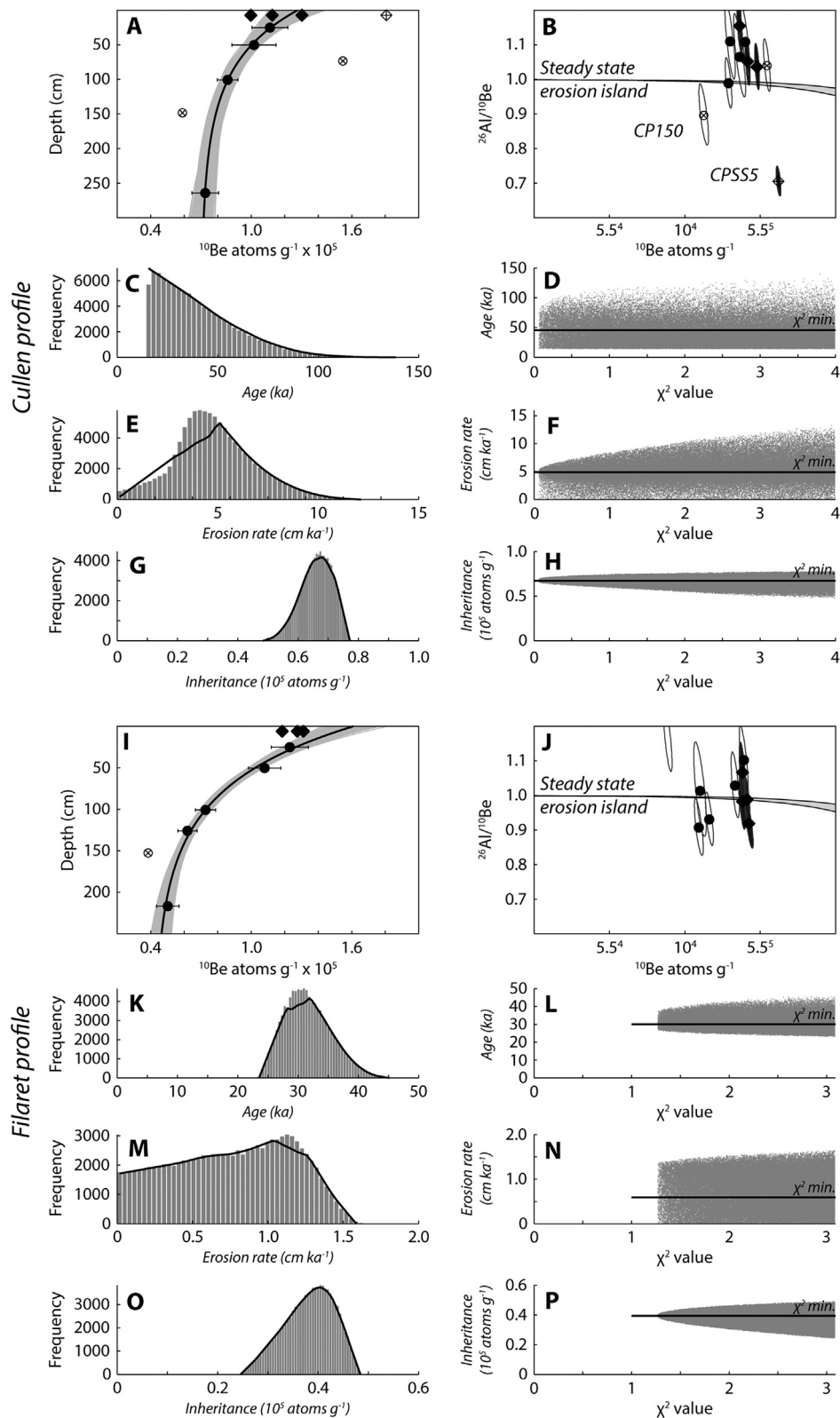
Fig. 4. Cosmogenic nuclide and modelling results for the depth and surface samples from the Cullen profile (A–H) and Filaret profile (I–P). In A, B, I and J, circles are depth samples; diamonds are surface cobble samples; and crosses show excluded anomalies. A and I show results from 100,000 model runs (grey lines) and the optimum χ^2 profile (black line) through ^{10}Be depth samples, with ^{10}Be surface samples shown for reference. B and J show all samples as normalised ^{26}Al/^{10}Be ratios plotted against ^{10}Be concentration. The predicted range for a stable and steadily eroding surface is also shown (shaded area; Lal, 1991); samples plotting beneath this area may have undergone post-depositional shielding. C, E, G and K, M, O show the results of 100,000 ^{10}Be depth profile model runs for age, erosion rate (i.e. surface deflation) and inheritance respectively as frequency histograms (grey bars) and distributions (black lines) for both depth profiles. Likewise, D, F, H and L, N, P show these same 100,000 model runs as point clouds for age, erosion rate and inheritance against the χ^2 value for each model run, with the minimum χ^2 value overall indicated by a black line.

Table 3
Model parameters.

Parameter	Sensitivity tests		Unconstrained		4 m erosion		0.5 m erosion	
	Min.	Max.	Min.	Max.	Min.	Max.	Min.	Max.
Filaret profile ^{10}Be								
Density (g cm^{-3})	1	3	1	2.7	1	2.7	1	2.7
Age (ka)	0	5000	14.348	1100	14.348	1100	14.348	1100
Erosion rate (cm ka^{-1})	0	5	0	5	0	5	0	5
Total erosion (cm)	0	10,000	0	10,000	0	400	0	50
Inheritance (atoms,g^{-1})	0	200,000	0	180,000	0	180,000	0	180,000
Cullen profile ^{10}Be								
Density (g cm^{-3})	1	3	1	2.8	1	2.8	1	2.8
Age (ka)	0	4000	14.348	1100	14.348	1100	14.348	1100
Erosion rate (cm ka^{-1})	0	20	0	20	0	20	0	20
Total erosion (cm)	0	10,000	0	10,000	0	400	0	50
Inheritance (atoms g^{-1})	0	400,000	0	300,000	0	300,000	0	300,000
Other parameters								
Location (deg):	Filaret profile: −52.9743, −68.8310; Cullen profile: −52.8899, −68.4244							
Altitude (m.a.s.l.):	Filaret profile: 148 m; Cullen profile: 17 m							
Strike/dip (deg)	0				Depth of muon fit			5 m
Shielding	0.999999				Error in total production rate			0%
Cover	1				Sigma confidence level			2
^{10}Be half-life	1.387 (5% error)				# profiles			100,000
Scaling scheme	Stone (2000) after Lal (1991)				No parallelisation			
Reference production rate	3.74				Neutrons			160 ± 5

Table 4
^{10}Be depth sample modelling summary. The optimum values used are highlighted. Bayesian values cannot be used because χ^2 optimisation failed to reach a unique value.

	Filaret ^{10}Be profile								
	Unconstrained (100 m)			4 m			0.5 m		
	Age (ka)	Inheritance ($\times 10^4$ atoms g^{-1})	Erosion rate (cm ka^{-1})	Age (ka)	Inheritance ($\times 10^4$ atoms g^{-1})	Erosion rate (cm ka^{-1})	Age (ka)	Inheritance ($\times 10^4$ atoms g^{-1})	Erosion rate (cm ka^{-1})
Mean	582.5	2.18	2.93	80.1	3.4	2.31	31.6	3.82	0.76
Median	597.8	2.18	2.93	75.7	3.42	2.42	31.2	3.87	0.79
Mode	822.9	2.35	2.76	31.5	3.47	2.38	29.9	3.89	1.15
Optimum χ^2	35.5	3.84	1.25	34.6	3.92	1.11	**30.1**	**3.94**	**0.59**
Maximum χ^2	1100	4.81	4.14	206.8	4.86	4.04	**45.6**	**4.91**	**1.63**
Minimum χ^2	23.3	0	0	23.1	1.77	0	**23.1**	**2.43**	**0**
Bayesian most probable	37.9	2.35	2.77	37.9	3.52	2.45	26.1	3.91	1.14
Bayesian 2σ upper	1078.8	4.2	4.71	158.7	4.51	4.28	37.8	4.8	1.55
Bayesian 2σ lower	36.1	0.03	1.82	17.6	1.12	0.29	14.8	1.42	–

	Cullen ^{10}Be profile								
	Unconstrained (100 m)			4 m			0.5 m		
	Age (ka)	Inheritance ($\times 10^4$ atoms g^{-1})	Erosion rate (cm ka^{-1})	Age (ka)	Inheritance ($\times 10^4$ atoms g^{-1})	Erosion rate (cm ka^{-1})	Age (ka)	Inheritance ($\times 10^4$ atoms g^{-1})	Erosion rate (cm ka^{-1})
Mean	575.7	7.53	7.46	40.1	6.63	5.11	17.9	6.71	1.54
Median	590.5	7.29	7.18	35.7	6.66	4.95	17.5	6.75	1.59
Mode	559.6	6.49	6.29	17.3	6.71	4.5	14.9	6.71	1.73
Optimum χ^2	25.6	6.84	3.81	**45.6**	**6.73**	**4.87**	15.8	6.92	0.85
Maximum χ^2	1100	12.93	15.25	**139.9**	**7.81**	**13.28**	29.6	7.84	3.46
Minimum χ^2	14.3	3.84	0.03	**14.3**	**4.75**	**0**	14.3	4.9	0
Bayesian most probable	14.3	6.85	5.65	14.3	6.85	4.35	14.3	6.85	2.39
Bayesian 2σ upper	1074.6	10.74	13.24	87.9	7.47	10.4	24.7	7.47	3.25
Bayesian 2σ lower	25.7	4.88	3.63	NaN	5.28	0.45	–	5.36	–

4.2.5. Erosion rate

The erosion rate was unknown but sensitivity tests suggested it played no significant role in age determination (the *maximum total erosion* was always more important, see following sections), so we selected broad constraints throughout the model runs.

4.2.6. Maximum total erosion

The maximum total erosion is the total amount of surface erosion that the model will allow, and may limit the erosion rate over time if the threshold is low but the erosion rate is high. Sensitivity tests showed that the maximum total erosion strongly affected age outputs, but is an unknown. It was, therefore, the key determinant in constraining maximum modelled age.

4.2.7. Approach to modelling

To provide the most reliable estimates of age, erosion rate and inheritance from the depth profile modelling, we ran three models for each profile. Firstly, we ran the model 'unconstrained' using very wide parameter values from the χ^2 sensitivity tests. All of these parameters were essentially unrealistically wide (e.g. up to 100 m of erosion and 2.7 g cm^{-3} density) but this was useful to gauge if constraining the maximum total erosion altered the age results. Next, we constrained the maximum total erosion to 4 m to test whether there had been significant surface deflation similar to the moraine exhumation of Kaplan et al. (2007), and then 0.5 m, which is more likely given field observations of preserved geomorphology and the tight clustering of surface cobble ages.
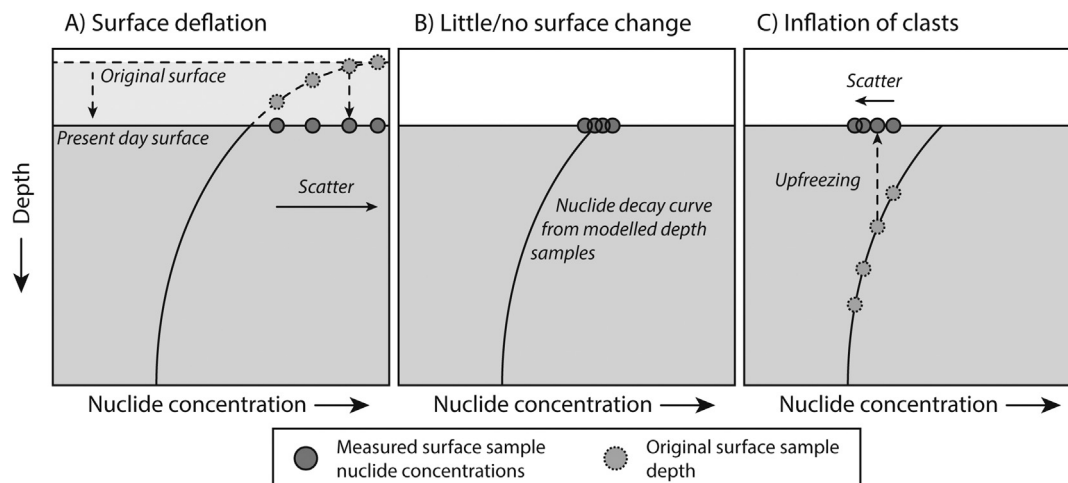
Fig. 5. An illustration of how geomorphic effects would be expected to alter the relationship between measured surface sample nuclide concentrations and the modelled nuclide decay curve from depth samples. The three diagrams show cosmogenic nuclide concentrations increasing towards the right and depth increasing towards the bottom. The nuclide decay curves, sample concentrations and depths are purely hypothetical. (A) Deflation of the outwash surface will result in surface cobbles that were within the original surface being uncovered at the present day surface. Such samples will show a scatter of nuclide concentrations greater than that modelled for the unit from the depth samples. (B) Little or no surface processes will result in accordance between surface samples and the modelled nuclide concentration for the unit, with the former showing little or no scatter. (C) Inflation of the surface samples due to processes such as upfreezing will raise cobbles to the surface, such that the surface samples will show a scatter of nuclide concentrations lower than that modelled for the unit from the depth samples.

Total erosion of the profile is a key parameter, and modelling shows that a minimum of ∼4 m of moraine exhumation is required to have artificially reduced the ages of corresponding moraine boulders (Kaplan et al., 2007). However, a maximum of 0.5 m of outwash surface deflation is more likely given: (1) the surface cobble samples are susceptible to deflation, but do not show scattered ages as would be expected if surface lowering had occurred (Fig. 5; Hein et al., 2011); (2) the preservation of braided meltwater channels is not consistent with several metres of surface deflation. Consequently, we constrained the maximum total erosion parameter (i.e. outwash surface deflation) within these two hypothetical scenarios, and applied conservative constraints to all other modelling parameters according to sensitivity tests. A consequence of this conservative approach is wider age uncertainties, and only optimum χ^2 values are given with ≥95% confidence (see Hidy et al., 2010 for discussion).

4.3. Depth profile modelling results

The modelled Río Cullen profile yielded a ^{10}Be age of 45.6 ka ($+139.9/-14.3$) when constrained to a maximum of 4 m of surface deflation (Fig. 4). Allowing 0.5 m of deflation created a stratigraphic age reversal younger than the gLGM. This is unrealistic compared to regional radiocarbon ages (Hall et al., 2013; McCulloch et al., 2005b) and suggests that some (>0.5 m) surface deflation has affected the age estimate. However, even with an unrealistic 100 m of deflation, the optimum age remained below 50 ka. The model yielded an erosion rate of 48.7 mm ka^{-1} (equating to 2.2 m of apparent erosion after 45.6 ka) and a low inheritance signature of 6.73×10^4 atoms g^{-1}. The San Sebastián profile yielded a ^{10}Be age 30.1 ka ($+45.6/-23.1$) when constrained to 0.5 m of deflation (Fig. 4) and, again, even allowing for 100 m of deflation, the optimum age remained below 50 ka. The model yielded an erosion rate of 0.59 mm ka^{-1} (equivalent to 0.2 m of apparent erosion after 30.1 ka) and a low inheritance signature of 3.94×10^4 atoms g^{-1}.

5. Discussion

The depth profile and surface sample ages for the outwash associated with the Río Cullen and San Sebastián glacial limits suggest that these surfaces are substantially younger than previously thought. For the depth profiles, the optimum ages are 45.6 ka ($+139.9/-14.3$) for the Río Cullen limit and 30.1 ka ($+45.6/-23.1$) for the San Sebastián limit (Fig. 4). The surface samples yield apparent mean ages of 27.2 ± 3.7 ka for the Río Cullen limit and 25.9 ± 1.3 for the San Sebastián limit, which suggests that there has not been substantial deflation of the outwash surfaces that would otherwise result in a scatter of ages. Moreover, the depth profiles and the surface samples are consistent with published dates from moraine boulders (Fig. 6), which were previously hypothesised to be poor estimates of moraine age due to erosion (Kaplan et al., 2007). Rather, we show that the Río Cullen and San Sebastián limits were deposited during the last glacial cycle (MIS 4-2), with optimum ages during MIS 3. These new constraints radically alter the glacial chronology of the BI-SSb lobe and demonstrate that it was more extensive during the last glacial cycle, but prior to the gLGM.

As noted, high moraine exhumation and boulder erosion rates have been invoked to suggest that exposure ages from moraine boulders on these glacial limits underestimated their age (Kaplan et al., 2007). Our data suggests surface deflation rates of 48.7 mm ka^{-1} and 0.59 mm ka^{-1} for the Río Cullen and San Sebastián outwash, respectively. The former is relatively high because the age and erosion rates are not well constrained, which is due to fewer samples and our conservative modelling constraints. In contrast, the San Sebastián outwash age and deflation rate estimates are well-constrained. Crucially, all modelled erosion rates are substantially lower than those required for the limits to be hundreds of thousands of years old (Meglioli, 1992), and the close agreement of the depth and surface ages suggests that deflation has not substantially lowered our ages.

5.1. Geomorphic considerations

Our modelling does not support erosion rates consistent with the loss of metres of surface sediment that might be expected if significant deflation of the outwash surface has occurred. However, our erosion rates are assumed to be steady over time, and do not consider rapid, episodic erosion (Kaplan et al., 2007). There are three reasons why we believe that high rates of episodic exhumation and erosion has not occurred. First, mass stripping of the outwash surfaces should have caused deflation of surface cobbles.
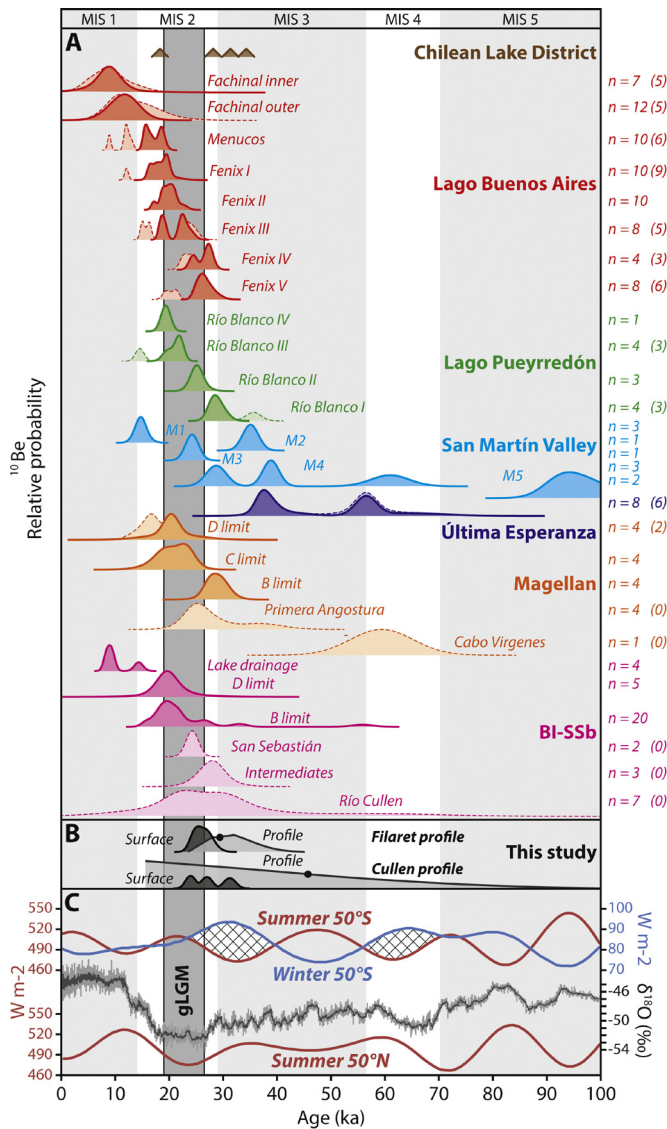
Fig. 6. (A) Published dating of selected former ice lobe advances over the last 100 ka in Patagonia from north to south, with MIS limits (light grey bars) from Lisiecki and Raymo (2005) and the LGM (dark grey bar) from Clark et al. (2009). For each location except the Chilean Lake District radiocarbon dates, all moraine boulder ^{10}Be data are shown as cumulative probability density function plots normalised to 1 (n = no. of samples). All dates have been recalculated, but note that: the number of samples varies between sites; no erosion or geomorphic processes have been considered; and some data have been truncated at 100 ka (see Supplementary Material). Lighter plots with dashed lines indicate all dates (normalised), whereas darker plots with solid lines have had outliers removed that were identified in the original studies (again, normalised). (B) Surface cobble (dark shading) and depth profile (light shading) results for the BI-SSb lobe from this study shown as cumulative probability density function plots, with the black dots indicating the optimum ages for each modelled profile. (C) Insolation data (Berger and Loutre, 1991) and the δ^{18}O record, with 10-pt moving average, from Dronning Maud Land (EPICA, 2006). Hatching in the southern insolation curves highlights times of low summer insolation and high seasonality during MIS 4-2.

However, the surface cobble sample ages are relatively tightly clustered, suggesting that surface deflation is unlikely (Fig. 5). Our sensitivity tests showed that a maximum χ^2 age of 350 ka (MIS 10) for the Filaret profile required ~6.4 m of erosion and a maximum χ^2 age of 450 ka for the Cullen profile required ~17 m of erosion. This is unlikely given the tight clustering of surface cobble ages. Secondly, the exceptionally high erosion rates associated with exhumation and erosion of the moraine boulders would likely have destroyed the glacial geomorphology, including the kettle kame topography and braided meltwater channels on the outwash plains.

The preservation of geomorphology suggests that this was not the case. Finally, intense erosion to artificially reduce the ages of the exhumed moraine boulders associated with the San Sebastián and Río Cullen glacial limits should also have affected boulders associated with the Bahía Inútil glacial limit. However, the Bahía Inútil limit is independently dated to the gLGM using other dating techniques and the Bahía Inútil boulders yield consistent cosmogenic nuclide ages. It is possible that intense erosion only took place during a short period after exhumation of the San Sebastián and Río Cullen boulders and before the gLGM and deposition of the Bahía Inútil boulders (Kaplan et al., 2007), but that still does not account for the preservation of the other glacial geomorphology.

5.2. Comparison to other glacial chronologies

Our BI-SSb chronology is unusual because none of the preserved glacial limits of the BI-SSb lobe pre-date the last interglacial (MIS 5) and two major limits were deposited during MIS 3, ~100 km beyond the gLGM limit (Fig. 1; Kaplan et al., 2008; McCulloch et al., 2005b). The precise extent of the offshore limits is unclear (Fig. 1; Rabassa, 2008), but the onshore limits demonstrate a markedly different pattern to northern Patagonia, where nested glacial limits were deposited during progressively less extensive glaciations over hundreds of thousands of years (Hein et al., 2009; 2011; Kaplan et al., 2005). Other pre-gLGM glacial advances have been recorded at a similar time during the last glacial cycle in Patagonia, but none are as extensive (Fig. 6). Glasser et al. (2011) reported ages of ca. 34–38 ka, 61 ka and ≥99 ka for limits of the San Martín valley lobe (49°S), and Sagredo et al. (2011) found ages of ca. 37–39 ka and 61 ka for the Última Esperanza lobe (52°S) in southern Patagonia (see Fig. 1 for locations). In northern Patagonia, Hein et al. (2010) found ages of 27–32 ka for the Lago Pueyrredón valley lobe (47.5°S), and Denton et al. (1999) suggested that glacial advances occurred by ≥34 ka in the Chilean Lake District (41–43°S). Elsewhere in the southern mid-latitudes Rother et al. (2014) found an age of ca. 28 ka for moraines of the Rangitata glacier (43°S), and Putnam et al. (2013) and Kelley et al. (2014) reported ages of ca. 33 ka and as early as ca. 43 ka, respectively, for pre-gLGM moraines of the Ohau glacier and Pukaki glacier (44°S) in the Southern Alps of New Zealand. These advances correlate with other pre-gLGM ages in New Zealand, Australia and Tasmania and support the assertion that, globally, not all ice sheets reached their maximum extents at the gLGM during the last glacial cycle (Hughes et al., 2013). Notably, however, these published advances for MIS 3 glaciation across the southern mid-latitudes were only slightly more extensive than their respective LGM limits. Our study supports the occurrence of MIS 3 glaciation, but also suggests that this was much more extensive in southernmost Patagonia than elsewhere.

Without further chronological controls on southern ice lobes, it is not possible to discount internal dynamic processes (e.g. surging) of the BI-SSb lobe as the cause of the MIS 3 glacial advances. However, if the lobe is representative of southernmost Patagonia, then an external forcing likely triggered glacial advance. The consistent occurrence of an MIS 3 advance across the southern mid-latitudes coincides with minimum summer insolation at ca. 32.5 ka in the southern hemisphere; in the northern hemisphere, the summer insolation minimum coincided with the gLGM (Fig. 6). Southern winter insolation also peaked at ca. 32.5 ka, and the combination of cooler summers and warmer winters may have promoted ice expansion prior to the coldest global temperatures during the gLGM. That said, the uncertainty in the age of the Río Cullen limit does not preclude the possibility that it was deposited during the previous summer insolation minimum/winter insolation maximum at ca. 61.5 ka. Season duration has been suggested as a

greater control on southern hemisphere climate than insolation intensity (Huybers and Denton, 2008), so winter duration may help to account for MIS 3 advances, given the trend toward longer winters during MIS 3 (Putnam et al., 2013). Furthermore, Putnam et al. (2013) interpreted pre-gLGM advances of the Ohau glacier in New Zealand as having resulted from the build-up of Southern Ocean sea ice during longer winters, inducing ocean stratification and cooling equivalent to the gLGM. Kelley et al. (2014) suggested that such temperatures may have been induced by cool events in Antarctica, propagated across the southern mid-latitudes via the ocean and/or atmosphere from at least 42 ka.

These mechanisms may help to explain the glacial advances during MIS 3 in southernmost Patagonia, but the significantly more extensive nature of the BI-SSb lobe compared to other records (e.g. Kelley et al., 2014; Putnam et al., 2013; Rother et al., 2014) requires an additional explanation. One possibility is that the extensive pre-gLGM advance was caused by increased ice accumulation due to increased precipitation. Rother et al. (2014) suggested that persistently greater levels of precipitation were necessary to create pre-gLGM advances similar to those during the gLGM across the southern mid-latitudes. Moreover, Kerr and Sugden (1994) demonstrated that Patagonian glaciers were latitudinally sensitive to precipitation south of 50°S, and it is possible that a southward shift in the Southern Westerly Winds delivered particularly high levels of precipitation to the BI-SSb lobe during MIS 3. This would have triggered significantly greater accumulation over southernmost Patagonia and a more extensive glacial advance than further north in Patagonia and New Zealand. Ultimately, without greater constraint on other glacial chronologies, the precise forcing of extensive, pre-gLGM advances in southernmost Patagonia remains unclear.

6. Conclusions

Cosmogenic nuclide dating of depth profiles through outwash sediments demonstrate that two limits of the BI-SSb lobe on Tierra del Fuego previously ascribed to MIS 12 and 10 relate to the last glacial cycle, between MIS 4 and 2. The San Sebastián limit was deposited at *ca.* 30.1 ka, suggesting that there was an MIS 3 glacial advance when the BI-SSb lobe was significantly more expansive than at the gLGM. The Río Cullen limit is not as well constrained but was likely deposited at *ca.* 45.6 ka and not before 139.9 ka. The results indicate extensive glaciation in southernmost Patagonia during MIS 3, which we interpret to reflect increased precipitation at this time, compared to the gLGM.

Acknowledgements

Appendix A. Supplementary material

Supplementary material related to this article can be found online at http://dx.doi.org/10.1016/j.epsl.2015.07.030.

References

Balco, G., Stone, J.O., Lifton, N.A., Dunai, T.J., 2008. A complete and easily accessible means of calculating surface exposure ages or erosion rates from [10]Be and [26]Al measurements. Quat. Geochronol. 3, 174–195.

Berger, A., Loutre, M.F., 1991. Insolation values for the climate of the last 10 million years. Quat. Sci. Rev. 10, 297–317.

Bujalesky, G., Coronato, A., Isla, F., 2001. Ambientes glacifluviales y litorales Cuaternarios de la region del Rio Chico, Tierra del Fuego, Argentina. Rev. Asoc. Geol. Argent. 56, 73–90.

Caldenius, C., 1932. Las glaciaciones cuaternarias en la Patagonia y Tierra del Fuego. Geogr. Ann. 14, 1–164.

Clapperton, C.M., 1993. Quaternary Geology and Geomorphology of South America. Elsevier Science Publishers, B.V., Amsterdam.

Clapperton, C.M., Sugden, D.E., Kaufman, D.S., McCulloch, R.D., 1995. The last glaciation in central Magellan Strait, southernmost Chile. Quat. Res. 44, 133–148.

Clark, P.U., Dyke, A.S., Shakun, J.D., Carlson, A.E., Clark, J., Wohlfarth, B., Mitrovica, J.X., Hostetler, S.W., McCabe, A.M., 2009. The Last Glacial Maximum. Science 325, 710–714.

Codignotto, J.O., Malumian, N., 1981. Geologia de la region al Norte de Paralelo 54S de la Isla Grande de Tierra del Fuego. Rev. Asoc. Geol. Argent. XXXVI VI, 44–51.

Coronato, A., Martínez, O., Rabassa, J., 2004. Glaciations in Argentine Patagonia, southern South America. In: Ehlers, J., Gibbard, P.L. (Eds.), Developments in Quaternary Sciences. Elsevier, pp. 49–67.

Darvill, C.M., Bentley, M.J., Stokes, C.R., 2015. Geomorphology and weathering characteristics of Erratic Boulder Trains on Tierra del Fuego, southernmost South America: implications for dating of glacial deposits. Geomorphology 228, 382–397.

Darvill, C.M., Stokes, C.R., Bentley, M.J., Lovell, H., 2014. A glacial geomorphological map of the southernmost ice lobes of Patagonia: the Bahía Inútil – San Sebastián, Magellan, Otway, Skyring and Río Gallegos lobes. J. Maps 10, 500–520.

Denton, G.H., Lowell, T.V., Heusser, C.J., Schlüchter, C., Andersen, B.G., Heusser, L.E., Moreno, P.I., Marchant, D.R., 1999. Geomorphology, stratigraphy, and radiocarbon chronology of Llanquihue Drift in the area of the Southern Lake District, Seno Reloncaví, and Isla Grande de Chiloé, Chile. Geogr. Ann., Ser. A, Phys. Geogr. 81, 167–229.

EPICA, 2006. One-to-one coupling of glacial climate variability in Greenland and Antarctica. Nature 444, 195–198.

Evenson, E.B., Burkhart, P.A., Gosse, J.C., Baker, G.S., Jackofsky, D., Meglioli, A., Dalziel, I., Kraus, S., Alley, R.B., Berti, C., 2009. Enigmatic boulder trains, supraglacial rock avalanches, and the origin of "Darwin's boulders," Tierra del Fuego. GSA Today 19, 4–10.

Glasser, N.F., Jansson, K.N., Goodfellow, B.W., de Angelis, H., Rodnight, H., Rood, D.H., 2011. Cosmogenic nuclide exposure ages for moraines in the Lago San Martín Valley, Argentina. Quat. Res. 75, 636–646.

Hall, B.L., Porter, C.T., Denton, G.H., Lowell, T.V., Bromley, G.R.M., 2013. Extensive recession of Cordillera Darwin glaciers in southernmost Souther America during Heinrich Stadial 1. Quat. Sci. Rev. 62, 49–55.

Hein, A.S., Dunai, T.J., Hulton, N.R.J., Xu, S., 2011. Exposure dating outwash gravels to determine the age of the greatest Patagonian glaciations. Geology 39, 103–106.

Hein, A.S., Hulton, N.R.J., Dunai, T.J., Schnabel, C., Kaplan, M.R., Naylor, M., Xu, S., 2009. Middle Pleistocene glaciation in Patagonia dated by cosmogenic-nuclide measurements on outwash gravels. Earth Planet. Sci. Lett. 286, 184–197.

Hein, A.S., Hulton, N.R.J., Dunai, T.J., Sugden, D.E., Kaplan, M.R., Xu, S., 2010. The chronology of the Last Glacial Maximum and deglacial events in central Argentine Patagonia. Quat. Sci. Rev. 29, 1212–1227.

Hidy, A.J., Gosse, J.C., Pederson, J.L., Mattern, J.P., Finkel, R.C., 2010. A geologically constrained Monte Carlo approach to modeling exposure ages from profiles of cosmogenic nuclides: an example from Lees Ferry, Arizona. Geochem. Geophys. Geosyst. 11, Q0AA10.

Hughes, P.D., Gibbard, P.L., Ehlers, J., 2013. Timing of glaciation during the last glacial cycle: evaluating the concept of a global 'Last Glacial Maximum' (LGM). Earth-Sci. Rev. 125, 171–198.

Huybers, P., Denton, G., 2008. Antarctic temperature at orbital timescales controlled by local summer duration. Nat. Geosci. 1, 787–792.

Kaplan, M.R., Coronato, A., Hulton, N.R.J., Rabassa, J.O., Kubik, P.W., Freeman, S.P.H.T., 2007. Cosmogenic nuclide measurements in southernmost South America and implications for landscape change. Geomorphology 87, 284–301.

Kaplan, M.R., Douglass, D.C., Singer, B.S., Caffee, M.W., 2005. Cosmogenic nuclide chronology of pre-last glacial maximum moraines at Lago Buenos Aires, 46°S, Argentina. Quat. Res. 63, 301–315.

Kaplan, M.R., Fogwill, C.J., Sugden, D.E., Hulton, N., Kubik, P.W., Freeman, S.P.H.T., 2008. Southern Patagonian glacial chronology for the Last Glacial period and implications for Southern Ocean climate. Quat. Sci. Rev. 27, 284–294.

Kaplan, M.R., Hein, A.S., Hubbard, A., Lax, S.M., 2009. Can glacial erosion limit the extent of glaciation? Geomorphology 103, 172–179.

Kaplan, M.R., Strelin, J.A., Schaefer, J.M., Denton, G.H., Finkel, R.C., Schwartz, R., Putnam, A.E., Vandergoes, M.J., Goehring, B.M., Travis, S.G., 2011. In-situ cosmogenic [10]Be production rate at Lago Argentino, Patagonia: implications for late-glacial climate chronology. Earth Planet. Sci. Lett. 309, 21–32.

Kelley, S.E., Kaplan, M.R., Schaefer, J.M., Andersen, B.G., Barrell, D.J.A., Putnam, A.E., Denton, G.H., Schwartz, R., Finkel, R.C., Doughty, A.M., 2014. High-precision [10]Be chronology of moraines in the Southern Alps indicates synchronous cooling in Antarctica and New Zealand 42,000 years ago. Earth Planet. Sci. Lett. 405, 194–206.

Kerr, A., Sugden, D., 1994. The sensitivity of the south Chilean snowline to climatic change. Clim. Change 28, 255–272.

Lal, D., 1991. Cosmic ray labeling of erosion surfaces: in situ nuclide production rates and erosion models. Earth Planet. Sci. Lett. 104, 424–439.

Lisiecki, L.E., Raymo, M.E., 2005. A Pliocene–Pleistocene stack of 57 globally distributed benthic δ^{18}O records. Paleoceanography 20, PA1003.

McCulloch, R.D., Bentley, M.J., Tipping, R.M., Clapperton, C.M., 2005a. Evidence for late-glacial ice dammed lakes in the central Strait of Magellan and Bahia Inutil, southernmost South America. Geogr. Ann., Ser. A, Phys. Geogr. 87A, 335–362.

McCulloch, R.D., Fogwill, C.J., Sugden, D.E., Bentley, M.J., Kubik, P.W., 2005b. Chronology of the last glaciation in central Strait of Magellan and Bahia Inutil, southernmost South America. Geogr. Ann., Ser. A, Phys. Geogr. 87A, 289–312.

Meglioli, A., 1992. Glacial geology and chronology of southernmost Patagonia and Tierra del Fuego, Argentina and Chile. Geology, Lehigh.

Mercer, J.H., 1983. Cenozoic glaciation in the southern hemisphere. Annu. Rev. Earth Planet. Sci. 11, 99–132.

Nishiizumi, K., Imamura, M., Caffee, M.W., Southon, J.R., Finkel, R.C., McAninch, J., 2007. Absolute calibration of [10]Be AMS standards. Nucl. Instrum. Methods Phys. Res., Sect. B, Beam Interact. Mater. Atoms 258, 403–413.

Putnam, A.E., Schaefer, J.M., Barrell, D.J.A., Vandergoes, M., Denton, G.H., Kaplan, M.R., Finkel, R.C., Schwartz, R., Goehring, B.M., Kelley, S.E., 2010. In situ cosmogenic [10]Be production-rate calibration from the Southern Alps, New Zealand. Quat. Geochronol. 5, 392–409.

Putnam, A.E., Schaefer, J.M., Denton, G.H., Barrell, D.J.A., Birkel, S.D., Andersen, B.G., Kaplan, M.R., Finkel, R.C., Schwartz, R., Doughty, A.M., 2013. The Last Glacial Maximum at 44°S documented by a [10]Be moraine chronology at Lake Ohau, Southern Alps of New Zealand. Quat. Sci. Rev. 62, 114–141.

Rabassa, J., 2008. Late Cenozoic glaciations in Patagonia and Tierra del Fuego. In: Rabassa, J. (Ed.), Developments in Quaternary Sciences. Elsevier, pp. 151–204.

Rodés, Á., Pallàs, R., Braucher, R., Moreno, X., Masana, E., Bourlés, D.L., 2011. Effect of density uncertainties in cosmogenic [10]Be depth-profiles: dating a cemented Pleistocene alluvial fan (Carboneras Fault, SE Iberia). Quat. Geochronol. 6, 186–194.

Rodés, Á., Pallàs, R., Ortuño, M., García-Melendez, E., Masana, E., 2014. Combining surface exposure dating and burial dating from paired cosmogenic depth profiles. Example of El Límite alluvial fan in Huércal–Overa basin (SE Iberia). Quat. Geochronol. 19, 127–134.

Rother, H., Fink, D., Shulmeister, J., Mifsud, C., Evans, M., Pugh, J., 2014. The early rise and late demise of New Zealand's last glacial maximum. Proc. Natl. Acad. Sci. USA 111, 11630–11635.

Rutter, N., Schnack, E.J., Rio, J.d., Fasano, J.L., Isla, F.I., Radtke, U., 1989. Correlation and dating of Quaternary littoral zones along the Patagonian coast, Argentina. Quat. Sci. Rev. 8, 213–234.

Sagredo, E.A., Moreno, P.I., Villa-Martinez, R., Kaplan, M.R., Kubik, P.W., Stern, C.R., 2011. Fluctuations of the Última Esperanza ice lobe (52°S), Chilean Patagonia, during the last glacial maximum and termination 1. Geomorphology 125, 92–108.

Singer, B.S., Ackert, R.P., Guillou, H., 2004. ^{40}Ar/^{39}Ar and K–Ar chronology of Pleistocene glaciations in Patagonia. Geol. Soc. Am. Bull. 116, 434–450.

Stone, J.O., 2000. Air pressure and cosmogenic isotope production. J. Geophys. Res. 105, 23753–23759.

Sugden, D.E., Bentley, M.J., Fogwill, C.J., Hulton, N.R.J., McCulloch, R.D., Purves, R.S., 2005. Late-glacial glacier events in southernmost South America: a blend of 'northern' and 'southern' hemispheric climatic signals? Geogr. Ann., Ser. A, Phys. Geogr. 87A, 273–288.

Walther, A., Rabassa, J., Coronato, A., Tassone, A., Vilas, J.F., 2007. Paleomagnetic study of glacigenic sediments from Tierra del Fuego. In: GEOSUR Abstract Volume, p. 174.

Wastegård, S., Veres, D., Kliem, P., Hahn, A., Ohlendorf, C., Zolitschka, B., 2013. Towards a late Quaternary tephrochronological framework for the southernmost part of South America – the Laguna Potrok Aike tephra record. Quat. Sci. Rev. 71, 81–90.

Wilson, P., Bentley, M.J., Schnabel, C., Clark, R., Xu, S., 2008. Stone run (block stream) formation in the Falkland Islands over several cold stages, deduced from cosmogenic isotope ([10]Be and [26]Al) surface exposure dating. J. Quat. Sci. 23, 461–473.